The Physical and Chemical Nature of Technegas

Tim J. Senden, Klaus H. Moock, John Fitz Gerald, William M. Burch, Rodney J. Browitt, Christopher D. Ling and Graham A. Heath

Department of Physics, University College, University of New South Wales, Canberra; and Research School of Chemistry, Research School of Earth Sciences, and John Curtin School of Medical Research, and Australian National University, Canberra, Australia

Technegas, the discrete radio-aerosol particle, containing ^{99m}Tc has been investigated, and the chemical evolution and physical properties of the particle demonstrated. **Methods:** A commercial technegas generator was used to produce aerosols according to standard clinical procedures. The aerosols were collected by electrostatic precipitation and examined with transition electron microscopy (TEM), scanning electron microscopy (SEM) and force microscopy. The chemical evolution was examined by x-ray techniques and thermogravimetric analysis. **Results:** The active particle was identified as hexagonal platelets of metallic technetium contained within a thin layer of graphitic carbon. This composite structure is discussed in light of the metal particle behaving as a template for the carbon capsule. The average size of the observed hexagonal platelets, 30–60 nm, was only weakly dependent on the concentration of technetium in the crucible. **Conclusion:** The mechanism for the formation of the technegas particles has been developed and the particles involved characterized. It appears that the use of other metals also leads to the formation of similiar materials.

Key Words: technegas; lung; aerosol; technetium-99m-pertechnetate

J Nucl Med 1997; 38:1327–1333

Since its invention and first reported use in 1986 as a diagnostic radio-aerosol, technegas has been recognized as a major contributor to lung ventilation scintigraphy (*1*). More than 110 published citations are extant, many detailing its clinical effectiveness (*2,3*).

The great advantage in sensitivity afforded by the nature of radiotracers, in general, unfortunately also hinders the chemical identification of the discrete species which are generally present in only tiny quantities. It is, therefore, not surprising that, despite its medical importance, the exact physical and chemical nature of technegas remained unresolved. While several articles have been concerned mainly with particle size (*4–6*), there has also been speculation about the composition of the active species (*6,7*) and its formation (*8*). Only recently has there been a convincing observation of the active species in technegas (*9*).

The actual process of technegas formation discussed in this article is based on the chemistry and structure of the particle involved. In this context, both the liberated aerosol and the crucible residues were examined by transmission electron microscopy, atomic force microscopy and x-ray diffraction. Thermogravimetric analysis of $K^{99}TcO_4$ and graphite was performed to clarify which chemical species contributes to the formation of the aerosol and to identify the key reduction steps in the generation cycle. This led to the development of a proposed mechanism for the formation of technegas.

Although our focus is on the technetium-containing particles, other structurally similar metals, such as zinc, magnesium and rhenium, have been included. These hexagonally close-packed metals lend support to some of the observations concerning the structure of the technegas particle. Rhenium was also chosen for its chemical similarity to technetium.

MATERIALS AND METHODS

A standard technegas generator was used to produce all aerosols and crucible residues. The general procedure mirrored that we used clinically is as follows: the radio tracer plus liquid carrier is evaporated to dryness in a graphite crucible, the simmer stage, which is then resistively heated in the burn stage to 2550°C for 15 sec in an atmosphere of pure argon. The temperature of the crucible was calibrated with an independent optical pyrometer. Ground state $K^{99}TcO_4$ in MilliQ water replaced the normal saline solution of $Na^{99m}TcO_4$ used in clinical production. The substitution of the Na-salt for K-salt does not represent a large chemical change. Indeed, under the conditions involved, the alkali metal cation cannot be expected to contribute to the final reduction process. This is presented in more detail below. About 0.1 ml of solution ranging in concentration from 10^{-2} to 5×10^{-6} mole L^{-1} was added to the crucible. The aerosol product was collected in each case by electrostatic precipitation (*10*) on a standard copper TEM grid supporting holey carbon films immediately after generation.

For the production of bulk crucible residues, $K^{99}TcO_4$ was also added in approximately milligram quantities to the crucible as a fine powder. After burns at milligram levels the crucibles were removed and the surface scraped with a scalpel to collect the dull gray residue coating the interior of the crucible. This procedure was performed under ethanol to minimize dispersal of the powder. The black powder was then transferred as a suspension to a quartz zero-background plate and moistened with 5% ethylene glycol in ethanol to act as a binder.

X-ray powder diffraction (XRD) of crucible residues was performed on a diffractometer using Cu Kα radiation with data aquistition of around 12 hr. The homologous rhenium complex, $KReO_4$, was investigated in the same manner as $K^{99}TcO_4$. Milligram quantities of zinc and magnesium metal (>99% BDH) were placed directly into the crucibles as small nuggets.

All aerosol and crucible residues were examined with transmission electron microscopy (TEM) capable of energy-dispersive x-ray analysis (EDXA). Scanning electron microscopy (SEM) of the crucible residues was performed on a unit equipped with a Robertson backscatter detector and light element EDXA.

Thermogravimetric analysis of an intimate mixture of $K^{99}TcO_4$ in an excess of spectroscopic grade graphite (1–2 μm particles, Aldrich) was performed in the temperature range 100-1300°C. Force microscopy was conducted in contact mode on a holey carbon grid under ambient conditions.

Received May 9, 1996; revision accepted Nov. 6, 1996.

For correspondence or reprints contact: Tim Senden, PhD, Dept. of Applied Mathematics, Research School of Physical Sciences and Engineering, Australian National University, Canberra, ACT, 0200, Australia.

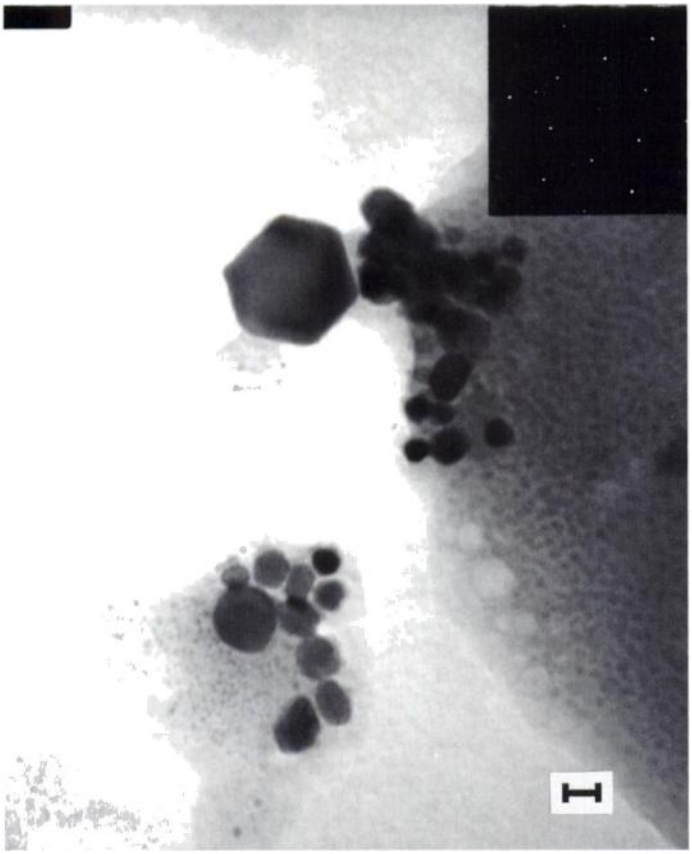

FIGURE 1. Transmission electron micrograph of a typical cluster of precipitated particles seen as near-perfect hexagonal platelets. Scale bar is 20 nm. Inset shows an electron diffraction pattern of a single platelet.

RESULTS

Aerosol Material

Figure 1 shows a transmission electron micrograph of a typical cluster of precipitated particles, seen as near-perfect hexagonal platelets. From TEM observations, particles larger than a few hundred nanometres were rare and most appeared to be less than 100 nm. This observation is typical for crucible loadings 3–4 orders higher than that used clinically. For loadings approaching clinical levels (still approximately 1 order higher) the center of the population distribution is around 30–60 nm in diameter. The ratio of the platelet thickness to diameter is around 1:10 in most cases. A typical particle is shown in Figure 2. Smaller particles were seen, however, direct identification from electron diffraction was difficult. Here the C-axis is perpendicular to the platelet plane.

Electron diffraction of the aerosol material, coupled with EDXA, proved conclusively that the primary technegas particle consists of the native metal. The inset in Figure 1 shows the diffraction pattern of a typical particle. The metallic aerosols deposited directly onto TEM grids demonstrate a remarkable resistance to aerial oxidation, in fact at no stage were any oxides or hydroxides observed. No evidence for the presence of TcC, a body-centered cubic phase with a_o = 0.3985 nm (*11*), was found in the aerosol output. Electron diffraction of the technetium platelets show lattice parameters of a_o = 0.274 (*5*) nm and c_o = 0.438 (*8*) nm, compared with the reported values of a_o = 0.27407 nm and c_o = 0.43980 nm (*12*).

Force microscopy of the surface of the technetium platelets revealed a covering with a layer of graphite. This is based on the resolution of the graphite lattice shown in Figure 3. This also confirms that the graphite (0001) planes are oriented parallel to the technetium surface. From TEM, some platelets showed the presence of a film but the graphitic lattice was not directly imaged.

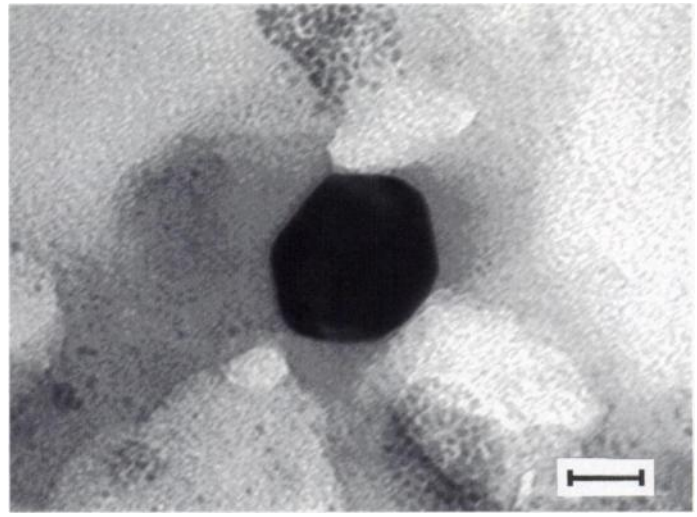

FIGURE 2. A typical particle of near-clinical level burn. Scale bar is 16 nm.

Crucible Residues

The crucible can be considered to be the heart of the generator, thus a description of its role in technegas production and its condition after production is crucial. SEM of the crucible residues remaining after a milligram-level burn is displayed in Figure 4. Because of the high conductivity of these samples, it was unnecessary to coat them with a conductive layer, such as gold or carbon. Energy dispersive x-ray analysis reveals that approximately half-micron-sized technetium-rich particles are distributed over the interior of the crucible with some concentration of material seen around the rim of the crucible. From EDXA, no elements other than technetium and carbon were detected. These technetium-rich particles can be seen at higher magnification in Figure 5A. Using backscattered electron imaging (Fig. 5B) the structure of the spherical particles can be seen to include a technetium-rich center, which is surrounded by carbon. The carbon shell is thin enough for the electrons to penetrate and scatter from the metal-rich center.

XRD data collected from the crucible residues is shown in Figure 6. With the exclusion of graphite peaks, all remaining

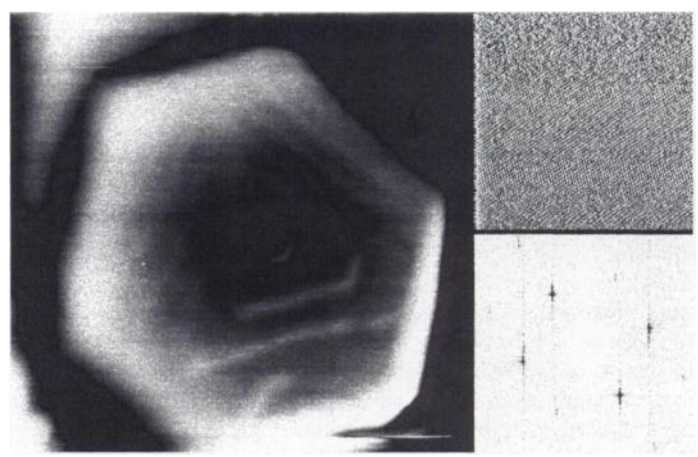

FIGURE 3. Force microscopy of the surface of a platelet precipitated onto a TEM grid showing a screw dislocation (image width is 500 nm). Inset on the top right is a closeup of the lattice on the surface of a more typical platelet (image width is 15 nm and is unfiltered). Lower right is the Fourier transform of the above lattice showing the same spacing and symmetry as the basal plane of graphite.

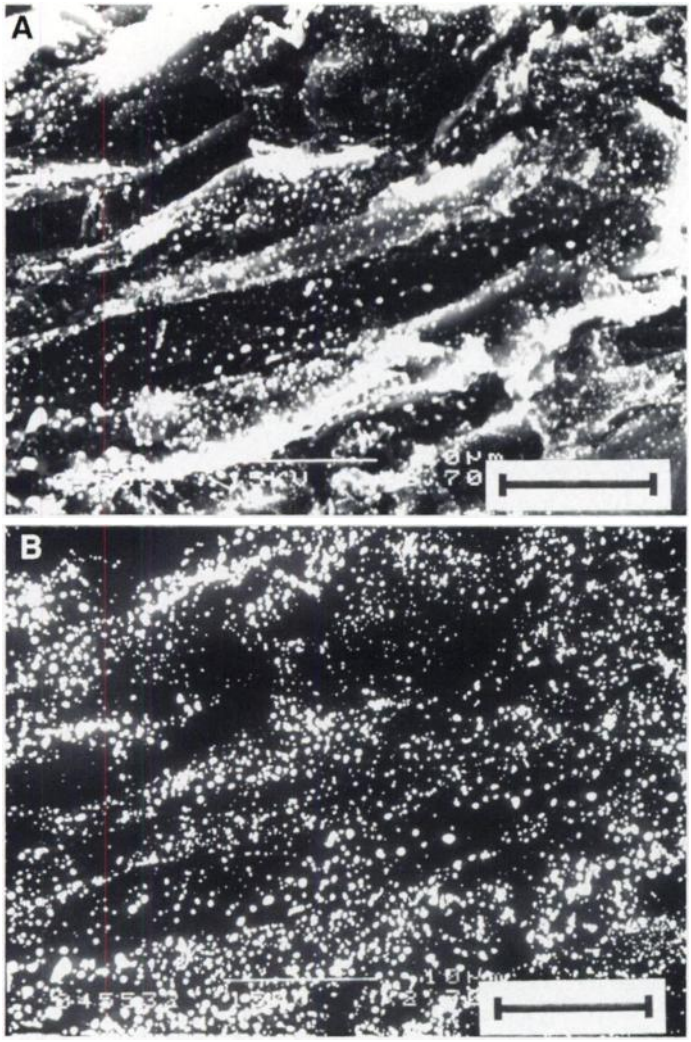

FIGURE 4. (A) Scanning electron micrograph of the crucible residues remaining after a milligram level burn. (B) Backscatter image of the same area. Scale bar is 10 μm.

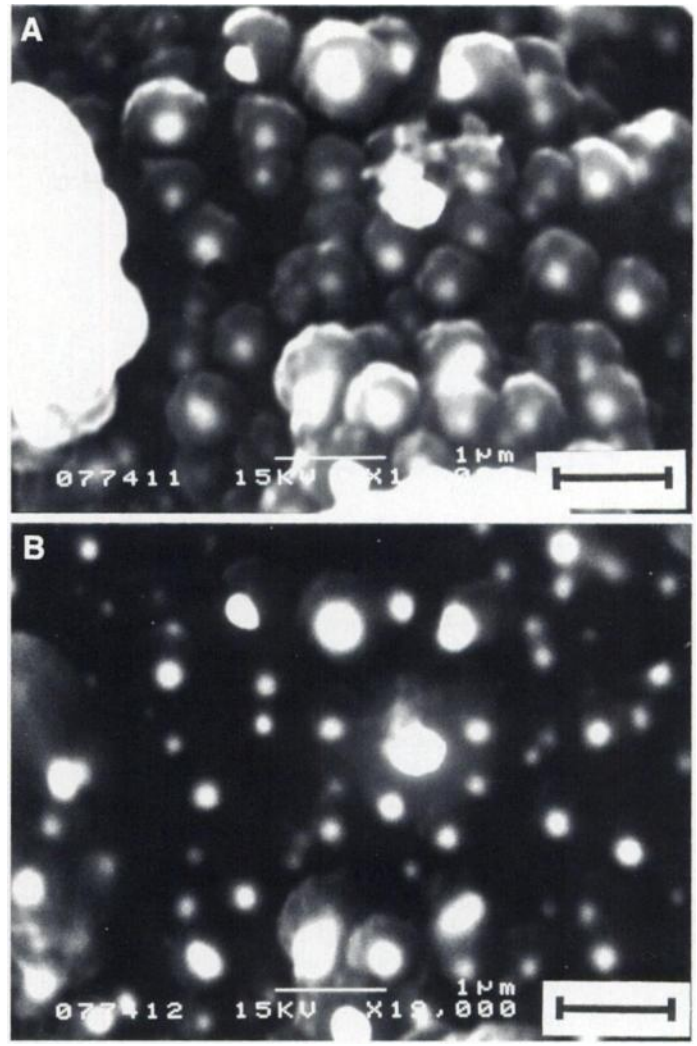

FIGURE 5. A detail of the crucible residues shown in Figure 4. (A) The technetium-rich particles can be seen in this secondary electron image. (B) Using backscattered electron imaging of the same area as A, the structure of the spherical particles can be demonstrated to include a technetium-rich center which is surrounded by carbon. Scale bar is 1 μm.

peaks within the 2θ range 5–125° were indexed to either technetium metal or TcC. There was no evidence for the existence of any technetium oxides or of the starting material, $K^{99}TcO_4$. Powder diffraction indicated approximately equal quantities of technetium metal and TcC. The first 10 reflections of each phase were matched within 0.004 nm (*13*), the technetium metal showing a slightly larger lattice parameter (~1.7%) indicating the possibility of carbon being incorporated within the lattice (*14*).

Figure 7 shows a transmission micrograph of some of the crucible residues dispersed in ethanol and cast onto a holey carbon TEM grid. Roughly spherical particles, some showing faceting, can be seen wrapped in graphitic layers. This is consistent with the SEM results, but reveals in more detail the structure of the encapsulating carbon.

Thermogravimetric Analysis

Figure 8 demonstrates the loss of mass as a function of temperature in a mixture of $K^{99}TcO_4$ and graphite under argon. Over the total temperature range a three-step mass loss occurs and by 1050°C all available $K^{99}TcO_4$ has been reduced to a mass equivalent to native technetium metal, with the loss of CO, CO_2 and KO_2 as gases. An overall reduction of the $K^{99}TcO_4$ can be formulated based on the equivalent mass loss, shown in the following equation:

$$2KTcO_4 + 3C \rightarrow CO_2\uparrow + 2CO\uparrow + 2KTcO_2 \rightarrow 2KO_2\uparrow + 2Tc.$$

The first reduction occurs over the interval 560–840°C, with the loss of CO and CO_2. Between 840°C and 1050°C, the mass loss of one equivalent per mol of KO_2 is observed.

Monitoring of Activity Release from the Crucible

The temperature at which the crucible liberates its activity into the gas phase was also studied. The activity of a crucible loaded with <1mCi of $Na^{99m}TcO_4$ was measured before and after a 15-sec burn at four precalibrated temperatures: 2150°C, 2380°C, 2430°C and 2550°C. Lower temperatures were not possible with the standard electronics configuration of the commercial generator. In addition, it should be noted that the error in the temperature measurement was ±50°C. The gamma activity of the crucible was determined using a proportional counter chamber. Figure 9A shows the percentage of the initial activity released into the gas phase after attaining a particular temperature. At 2100°C only 20% of activity is evolved, however, above 2350°C the release climbs rapidly with increasing temperature reaching >80% above 2550°C. This would, therefore, discount the simple sublimation of $KTcO_4$ [~1000°C (*15*)] as a mechanism for technegas evolution. In Figure 9B, a time series of activity profiles for a clinical burn sequence in a standard technegas generator is shown. It is seen that most of the activity does not leave the crucible (bottom of chamber)

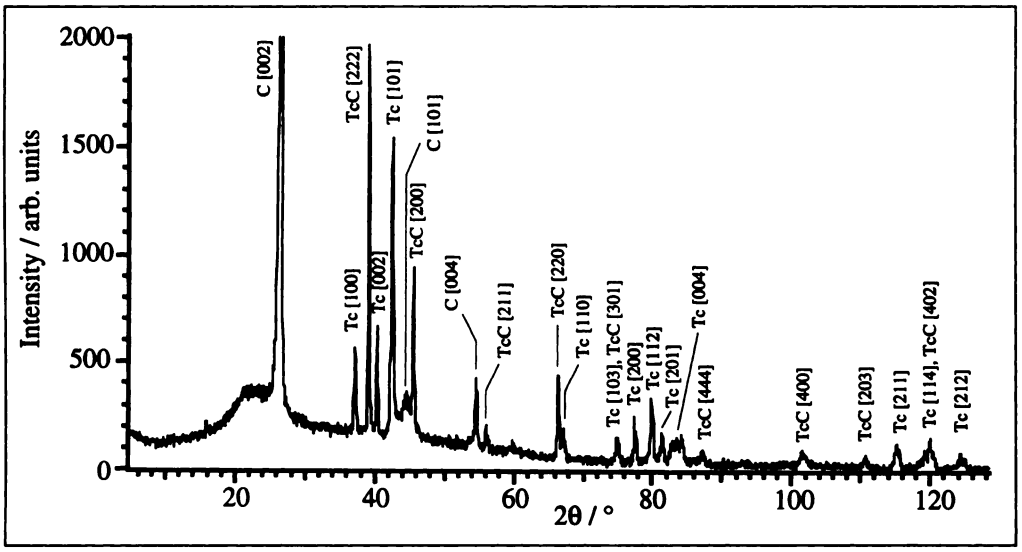

FIGURE 6. XRD data of material collected from a crucible after a milligram-level burn.

until the 1.0-sec mark. The specifications for the generator require that it reaches the full-burn temperature within the first 0.25 sec of operation. This would suggest that the component responsible for the evolution of the volatile active species has a vaporization point not far from the final crucible operating temperature. Hence, the lower melting point components such as NaCl and TcC do not appear to be major contributors to technetium evolution.

Other Metals

XRD analysis of the crucible residues formed from $KReO_4$ showed only the presence of the native metal. The lattice parameters were within error of reported values (*13*) and indicated no evidence for either the carbide or any oxides. Figure 10 shows an example of the crucible residues. Very little of the rhenium aerosol was found on the TEM grids after precipitation, occurring as irregular, facetted particles around 50 nm in diameter.

The aerosols produced from zinc and magnesium loadings were comprised entirely of ~100-nm hexagonal platelets, and exhibited the same inertness towards aerial oxidation as technetium. It should be noted that these metals, so finely divided, should be pyrophoric in air. Electron diffraction confirmed that these metals were retained in their native state. Details of this work will be presented elsewhere (*16*).

DISCUSSION

The formation and stabilization of the active particle in technegas is dependent on several factors: a chemical reductant, a volatile substrate and component, and surface passivation of the resultant aerosol. Figure 11 illustrates the proposed mechanism for technegas production.

The reduction of the pertechnetate to the native metal seems to proceed well before any aerosol is produced. The reduction by carbon occurs at the crucible interface, which is comprised of a fine sinter of micron-sized graphite particles. This begins at the melting point for $K^{99}TcO_4$, 540°C (*15*) when an intimate contact is formed between the molten $K^{99}TcO_4$ and the porous graphite. From TGA the first reduction occurs over the interval 560–840°C. The existence of the proposed Tc^{III} complex is supported by reports of the synthesis of an isotypic sodium salt which has similar thermal stability (*17*). Interestingly, the loss of potassium in the second step requires an oxidation state change for oxygen in the decomposition of the $KTcO_2$. That is, the two $[O^{2-}]$ moieties act together as a three-electron reductant for the Tc^{3+} forming the superoxide $[O_2]^{-1}$ and leading to the volatile KO_2 species.

At temperatures above the melting point for Tc, 2250 ± 50°C (*18*), the vapor pressure of the metal will increase significantly. Once in the vapor phase, technetium can condense and collect in the chamber as a metallic aerosol. Under these conditions the technetium particles form near perfect, thin hexagonal platelets, a consistent morphology considering the hcp structure. The

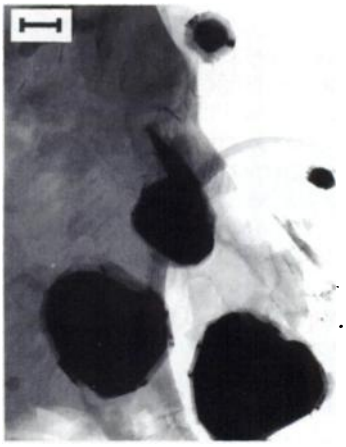

FIGURE 7. Transmission electron micrograph of technetium-containing crucible residues dispersed in ethanol and cast onto a holey carbon grid. Scale bar is 50 nm.

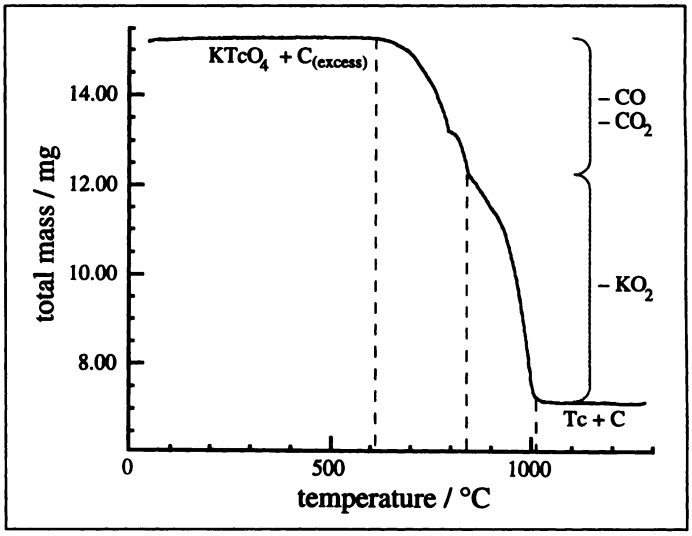

FIGURE 8. Thermogravimetric analysis of a mixture of $K^{99}TcO_4$ and graphite (excess).

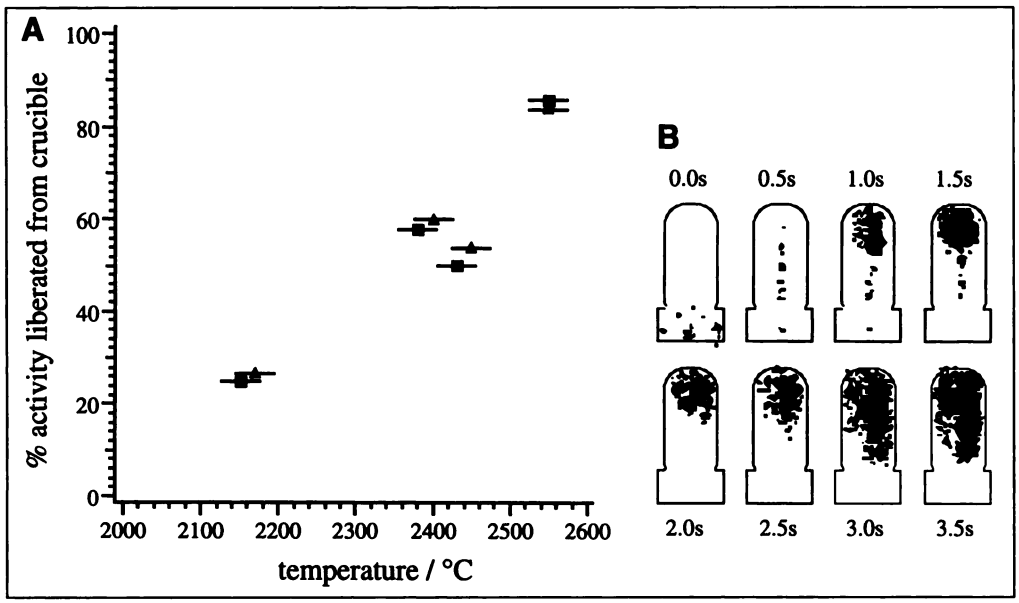

FIGURE 9. (A) Relationship between the percentage of activity to leave the crucible is plotted as a function of temperature. The data were obtained by electrostatically collecting the gaseous output from the generator and then counting this in a scintillation pot. Dilute doses of clinical ^{99m}Tc solution in saline were used. (B) A time series of activity profiles for a clinical burn sequence in a standard technegas generator. Each frame is separated by 0.5 sec and the cross-section of the chamber is outlined. The crucible comes up to full temperature, around 2550°C, in the first 0.25 sec of operation.

initial condensation would be likely to occur very close to the crucible because of the extreme temperature gradients.

Occurring simultaneously with the evaporation of technetium metal is the rapid increase in carbon vapor pressure. In the range 2000–3000°C the vapor pressure of graphite increases more than 6 orders of magnitude to around 70 mTorr for typical crucible temperatures (*19*). At this temperature, the hot carbon vapor exists largely as C_3 species (*19,20*) and will condense readily on any available cold surface. The significance of the recommended burn temperature of 2550°C is possibly due to the coincidence of appreciable rates of evaporation and sublimation of the technetium metal and graphite, respectively. Rapid sublimation of the crucible does not appear to be the main driving force for the ejection of the material, otherwise a larger proportion of TcC might be expected in the aerosol output. The retention of activity by the crucible after a burn is around 25% of the initial loading. Note that about half of the aerosol produced is available to the patient, the remaining aerosol collecting on the walls of the chamber during the 3-min cool-down period after a burn (*21*). The observation that activity only leaves the crucible at the melting point for technetium also indicates that the ejection mechanism is predominately a passive one, that is by evaporation of the metal.

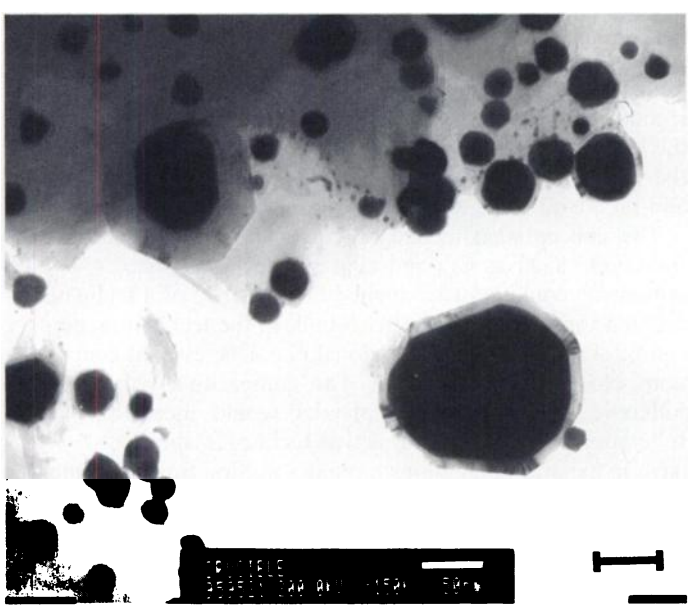

FIGURE 10. Transmission electron micrograph of rhenium-containing crucible residues dispersed in ethanol and cast onto a holey carbon grid. Scale bar is 50 nm.

The evidence obtained from the passivation of the native metallic aerosols for technetium, zinc and magnesium indicates that an impermeable layer of carbon has enclosed each particle. It is well known that most finely-divided metals oxidize rapidly in air and technetium is no exception (*18*). The ability of the carbon to encapsulate native metal was well demonstrated with the TEM and FM studies showing that the surface of the particles is at least partially ordered graphite. The effectiveness of the carbon to passivate the available metal surfaces at high crucible loadings indicates that there is ample carbon vapor present to coat the much smaller quantities of technetium present in clinical loads. The carbon film thickness varies, but rarely exceeds a few nanometers, as estimated by TEM images parallel to the platelet plane. Supporting evidence of a thin film also comes from force microscopy. The carbon, therefore, appears to form a coherent layer around the whole metal surface.

The encapsulation process would appear to occur after crystallization of the metallic aerosol. This is implied by comparison of the melting points of technetium, magnesium and zinc, with melting points of 2250°C, 650°C and 419°C, respectively. The crystallinity of both the metal and the carbon suggests that the two are at least commensurate over the plane of the particle [(0001) faces].

The participation of TcC in the mechanism of technegas formation is uncertain. It has been reported that above liquid TcC at 2300°C, at equilbrium, both TcC and technetium co-exist in the vapor phase (*22*). However, the vapor phase concentration of technetium is some 6 times higher than for TcC. From TEM studies, no strong evidence has been found for the condensation of TcC from the vapor phase, which may suggest a decomposition of TcC at the crucible operating temperatures (*11*). The other possibility is that the bulk of the TcC observed in the XRD forms on cooling of the crucible from the reservoir of technetium metal. The slow rate of TcC formation is supported by the published synthesis for the material (*11*).

A similar process occurs in the reduction of $KReO_4$. The paucity of aerosol for the rhenium burn might be attributed to

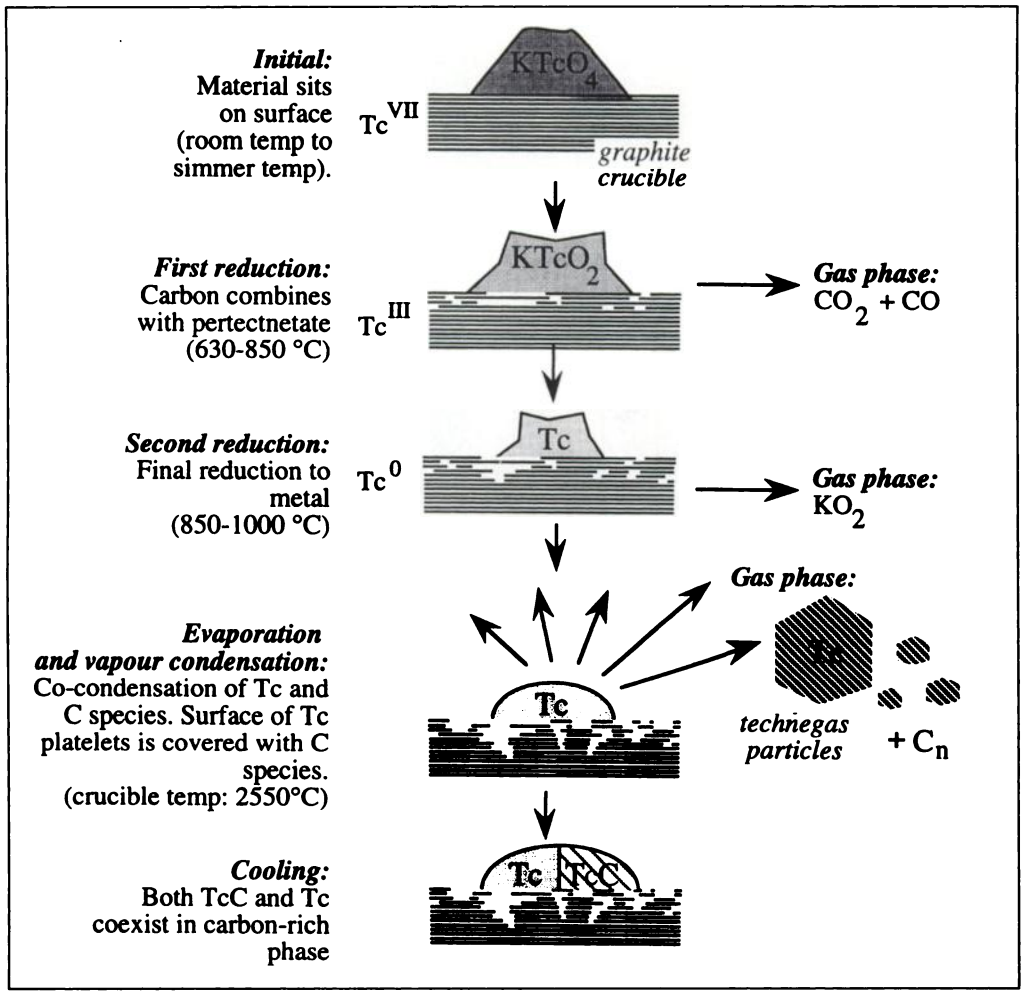

FIGURE 11. A schematic for the proposed mechanism of technegas production.

the high melting point of rhenium, 3180°C (*23*) resulting in a low vapor pressure under the prevailing burn temperature. The absence of ReC is not surprising as it has been reported to decompose to a metal-carbon mixed phase at atmospheric pressure above 1500°C (*24*).

The saline found in the clinical stock was deliberately omitted from runs performed in this work. Aerosols collected from burns from clinical pertechnetate solutions were overloaded with NaCl crystals, which obscure all imaging procedures. Evidence from the lift-off studies of the burn cycle show that, at temperatures where NaCl evaporates, no significant activity is ejected. Hence, it was concluded that NaCl played no part in the primary technegas particle evolution.

In chemical terms, the quantities of technetium used in a typical clinical production of the technegas are approaching the detection limits for analytical techniques. The need to scale up the quantities of material, in order to aid identification raises the concern that the product may change form. It should be noted that the same particle structure, hexagonal platelets, was observed over all concentration ranges, ~50 ng to ~1,000,000 ng. At the 50-ng level, the technetium concentration was close to the approximately 1–10 ng found in clinical runs, while still being detectable with the methods used in this study. In unusual cases clinical loading may be as high as 200 ng, although specific activity might be low (Forrest TRF, *personal communication*, 1986).

While the chemical processes are not altered by increasing the crucible loading above the clinical level, it is the physics of encapsulation that requires careful consideration. It was observed that, at loadings nearly three orders of magnitude higher than clinical use, the output of the technegas was unaffected (Forrest TRF, *personal communication*, 1986). It appears that over the whole range of crucible loadings sufficient carbon vapor is produced to protect all exposed aerosol interfaces.

The average particle size, at close to clinical loading, was around 30–60 nm in width and around 5 nm in thickness, with 80% of particles being below 100 nm. The platelet size seemed to be a relatively weak function of crucible loading with platelets rarely exceeding 500 nm in width even at the highest crucible loadings. Given the high rate of evaporation and low technetium vapor pressure, particle size should be controlled by the rate of cooling. In the time the metallic vapor condenses to the solid metal, a loss of only 300°C, few collisions are possible and the metal particle ceases to grow further.

The concept that technegas contains discrete radio-labeled fullerenes, such as C_{60} and C_{70}, has been suggested (*7*). Two arguments could be used against the presence of a technetium-fullerene species. First the great bulk of the technetium aerosol can be accounted for as hexagonal platelets, even at concentrations close to clincial loads. The comparitive volumes of a fullerene with an average platelet would mean that for a fullerene species to be the active technegas species, it would have to exist in populations around a million times the number of observed platelets. Second, the conditions are far from optimal for the efficient production of fullerenes (*25*).

It is worthwhile to compare and contrast the present carbon-encapsulated hexagonal platelets with fullerene structures and nanomeric carbon tubes. The platelets can be viewed as mesoscopic fullerenes, in which the graphite carbon skin forms a three-dimensional mesh over the seed metal particle (*16*). The

three-dimensional graphitic structure that forms around a nanocrystalline template is similar in structure and formation to that encountered by Saito et al. (*26,27*) enclosing iron and yttrium carbide.

Such a nanocolloidal structure reinforces the demonstrated biological inertness of technegas particles. On inhalation, the particles deposit well below the mucociliary escalator of the conducting airways. Indeed, lung imaging done up to 16 hr after inhalation has demonstrated particle loss to be <3% (Burch WM, *unpublished data*, 1995). If the particles are trapped from the argon carrier gas and ingested through water or food (such as rice), they travel the entire length of the gastrointestinal tract with no evidence of absorption up to 24 hr (*28*).

CONCLUSION

Technegas particles are hexagonal platelets of metallic technetium, each closely encapsulated with a thin layer of graphitic carbon. It appears that the key element to the successful operation of the technegas generator is the source of hot carbon. This provides both a chemical reductant and the means by which a passive film is deposited around the metallic aerosol to protect the condensed technetium metal from reoxidation. The other factor is that the crucible temperature is sufficiently high for rapid volatilization of both the technetium and the carbon. The resulting encapsulated aerosol can be regarded as a metal-bearing fulleremic material.

ACKNOWLEDGMENTS

We thank Dr. Ying Chen, David Llewellyn, Dr. Meta Sterns and Dr. Sally Stowe for their assistance and use of their facilities and Dr. Steve Geller for useful discussions. We thank Assoc. Prof. Dudley Creagh, and a federal government-sponsored research and development syndicate, arranged jointly by the National Australia Bank and Axiom R&D Management, for financial support.

REFERENCES

1. Burch W, Sullivan P, McLaren C. Technegas–a new ventilation agent for lung scanning. *Nucl Med Commun* 1986;7:865–871.
2. Murray IPC. Clinical experience with technegas. *Clin Nucl Med* 1991;16:247–250.
3. James JM, Testa HG. The use of ^{99m}Tc-technegas in the investigation of patients with pulmonary thromboembolism. *Nucl Med Commun* 1995;16:802–810.
4. Strong JC, Agnew JE. The particle size distribution of technegas and its influence on regional lung deposition. *Nucl Med Commun* 1989;10:425–430.
5. Lemb M, Oei TH, Eifert H, Gunter B. Technegas: a study of particle structure, size and distribution. *Eur J Nucl Med* 1993;20:576–579.
6. Lloyd JJ, Shields RA, Taylor CJ, Lawson RS, James JM, Testra HJ. Technegas and pertechnegas particle size distribution. *Eur J Nucl Med* 1995;22:473–476.
7. Mackey DWJ, Burch WM, Dance IG, Fisher KJ, Willett GD. The observation of fullerenes in a technegas lung ventilation unit. *Nucl Med Commun* 1994;15:430–434.
8. Scalzetti EM, Gagne GM. The transition from technegas to pertechnegas. *J Nucl Med* 1995;36:267–269.
9. Isawa T, Lee B-T, Hiraga K. High-resolution electron microscopy of technegas and pertechnegas. *Nucl Med Commun* 1996;17:147–152.
10. Browitt RD. A precipitator. 1995; Australian patent application #31778/95'.
11. Giorgi AL, Szklarz EG. Superconductivity of technetium and technetium carbide. *J Less Common Metals* 1966;11:455–456.
12. Marples JAC, Koch CC. Low temperature x-ray investigation of technetium and the technetium-molybdenum A-15 compound. *Phys Lett A* 1972;41:307–308.
13. King M, ed. *Powder diffraction file–inorganic phases*, vol. sets 1–44. xxxx: JCPDS, International Center for Diffraction Data; 1994:000–000.
14. Trzebiatowski W, Rudzinski J. On the existence of a technetium carbide. *Z Chem* 1962;2:158.
15. Anders E. Technetium and astatine chemistry. *Ann Rev Nucl Sci* 1959;9:203–220.
16. Senden TJ, Fitz Gerald J, Moock KH, et al. Ternary oxides of technetium oxidation states III to VII with alkaline metals. *J Inorg Nucl Chem* 1965;27:787–795.
17. Keller C, Kanellakopulos B, eds. Ternary oxides of technetium oxidation states III to VII with alkaline metals mit Alkalien. *J Inorg Nucl Chem* 1965;27:787–795.
18. Baptista de Alleluia I, Burgess J, Keller C, Möbius S, et al. Technetium. In: Kugler HK, Keller C, eds. *Gmelin handbook of inorganic chemistry*, vol. 2. Heidelberg: Springer-Verlag; 1993:214.
19. Leider HR, Krikorian OH, Young DA. Thermodynamic properties of carbon up to the critical point. *Carbon* 1973;11:555–563.
20. Pourbaix M, Yang X-Z, Zhang H-M. *Chemical and electrochemical equilibria in the presence of a gaseous phase*. Rapports techniques RT265. Brussels: Centre Belge d'Etude de la Corrosion; 1983:144.
21. *Technegas generator user manual*. 1993.
22. Rinehart GH, Behrens RG. Mass spectrometric determination of the dissociation energy of TcC(g). *J Phys Chem* 1979;83:2052–2053.
23. Weast RC. *CRC handbook of chemistry and physics*, 55th ed. Cleveland, OH: CRC Press; 1974.
24. Popova SV, Boiko LG. A new rhenium carbide formed by high-pressure treatment. *High Temp High Press* 1971;3:237–238.
25. Koch AS, Khemani KC, Wudl F. Preparations of fullerenes with simple benchtop reactor. *J Org Chem* 1991;56:4543–4545.
26. Saito Y, Yoshikawa T, Okuda M, et al. Iron particles nesting in carbon cages grown by arc discharge. *Chem Phys Lett* 1993;212:379–383.
27. Saito Y, Yoshokawa T, Okuda M, et al. Synthesis and electron-beam incision of carbon nanocapsules encaging YC_2. *Chem Phys Lett* 1993;209:72–76.
28. Burch WM, Browitt RD, Crellin D, Kanshik S. Technegas-labeled rice and water as physiological nonabsorbed gastric markers. *Jpn J Nucl Med* 1995;32:887.